Ocean Engineering 363 (2026) 126647

Contents lists available at ScienceDirect

Ocean Engineering

journal homepage: www.elsevier.com/locate/oceaneng

Research paper

Wave energy conversion using submerged piezoelectric plates with functionally graded graphene origami-enabled auxetic metamaterial substrates: A hydroelectromechanical study

Bill Murari [a,*], Zachary J. Wegert [b], Ben Wilks [c], Mergen H. Ghayesh [a], Ngamta Thamwattana [d], Vivien J. Challis [b], Michael H. Meylan [d]

[a] School of Electrical and Mechanical Engineering, Adelaide University, Adelaide, SA 5005, Australia
[b] School of Mathematical Sciences, Queensland University of Technology, Brisbane, QLD 4001, Australia
[c] School of Mathematical Sciences, Adelaide University, Mawson Lakes, SA 5095, Australia
[d] School of Computer and Information Sciences, University of Newcastle, Callaghan, NSW 2308, Australia

ARTICLE INFO

Keywords:
Wave energy conversion
Piezoelectric energy harvesting
Functionally graded metamaterials
Graphene origami
Hydroelectromechanical coupling

ABSTRACT

Ocean wave energy is a vast and largely under-used renewable resource with significant potential to contribute to the global transition away from fossil fuels. This study presents a theoretical investigation of wave energy conversion using submerged piezoelectric plates that incorporate a functionally graded graphene origami-enabled auxetic metamaterial (FG-GOEAM) substrate. A fully coupled hydroelectromechanical model is used based on Kirchhoff plate theory and linear potential flow, accounting for electromechanical coupling, fluid–structure interaction, and circuit dynamics. The governing equations are solved using a hypersingular boundary integral formation combined with a dry-mode expansion approach to capture diffraction, radiation, and scattering effects. We conducted a parametric analysis to examine how energy absorption is impacted by the folding degree and distribution of graphene origami, as well as the selection of piezoelectric materials, submersion depth, and support conditions. The findings demonstrate the potential of functionally graded graphene origami-enabled auxetic metamaterial substrates to tune the dynamic response of piezoelectric wave energy converters and offer insights into their role in improving energy harvesting performance.

1. Introduction

The global demand for renewable sources of energy is ever present, propelled by the desire to pivot away from traditional energy sources such as oil and coal. Fossil fuels currently supply approximately 80% of global energy demand (Singh, 2021), contributing to energy insecurity, environmental degradation, and adverse impacts on human health. The detrimental effects of these sources have been exhibited in the ecological imbalance of fauna and flora. As such, improving green and renewable energy is an effective way to ameliorate the energy crisis and improve the standard of living of the global population (Islam et al., 2022; Xu et al., 2022; Ramos et al., 2022). Renewable energy sources such as ocean wave energy and wind energy can be harnessed on a large scale. Specifically, ocean wave energy is relatively insensitive to variations in weather conditions and is available for exploitation while supplying clean and sustainable energy. In addition, wave energy has been reported to have the second-highest potential of ocean energy sources (Thorpe, 1999; Ilyas et al., 2014). One way to harness ocean wave energy is through the use of piezoelectric wave energy converters (PWECs) (Liu et al., 2023; Lian et al., 2024). PWECs convert mechanical energy to electrical energy via the piezoelectric effect of piezoelectric materials. Their high voltage output, efficiency, and simple design make them attractive solutions for their purpose. In general, wave energy converters (WECs) can be classified based on operational principles, wave propagation direction, distance from shore, and power take off (PTO). Within this broader classification, several notable piezoelectric harvesters have been reported in the literature, including small-scale piezoelectric wave energy harvesters operating on the acceleration-driven principle (Cai et al., 2022), piezoelectric coupled buoys to harness energy from ocean waves (Viet et al., 2016) and plate-wave energy converters moored in front of floating stationary breakwaters (Zheng et al., 2021; Qiao et al., 2020). As a result of their versatility and scalability, piezoelectric harvesting technology continues to receive significant research attention and offers a viable alternative to non-renewable energy sources, as well as a means of

* Corresponding author.
E-mail address: bill.murari@adelaide.edu.au (B. Murari).

https://doi.org/10.1016/j.oceaneng.2026.126647
Received 11 May 2026; Received in revised form 9 June 2026; Accepted 18 June 2026
Available online 25 June 2026

extracting power from the turbulent flow of oceans and seas (X.D. Xie et al., 2014). Despite the developments in this field, large-scale deployment in real marine environments remains a challenging endeavour (Chen et al., 2026; Li et al., 2024).

A piezoelectric energy harvester typically consists of a plate that incorporates one or two layers of piezoelectric material, referred to as unimorph and bimorph configurations, respectively (Erturk and Inman, 2008b). The harvester is attached to a vibrating structure, where the resulting dynamic deformations in the piezoelectric layers induce an alternating voltage across the electrodes, facilitating the conversion of energy from mechanical to electrical energy (Erturk and Inman, 2009; Erturk et al., 2010). Erturk and Inman (2008a) developed a distributed parameter electromechanical model for cantilevered unimorph and bimorph harvesters, using Euler–Bernoulli beam theory to analyse the effects of base motion and damping. It provides closed-form expressions for electrical output and explores the significance of electrode placement and strain nodes in enhancing energy harvesting efficiency. Kiran et al. (2020) reviewed recent advances in piezoelectric wave energy conversion technologies and demonstrated that flexible devices offer superior durability and power generation compared to their rigid counterparts. Their review highlighted the importance of specific piezoelectric effects (d_{33} and d_{15}) in enhancing energy output while integrating mathematical models to optimise design configurations. In addition, the necessary post-harvesting processes for effective energy management from harvested AC power are discussed. Na et al. (2018) studied a piezoelectric energy harvesting device that converts wave kinetic energy into electrical energy through the impact force exerted on a bimorph piezoelectric element. The multiphysical analysis aimed at optimising performance through the configuration of its components, including a triple-layer piezoelectric bender, thus enhancing energy capture from wave motion. Renzi (2016) studied the hydroelectromechanical dynamics of a piezoelectric wave energy converter, which consisted of a flexible bimorph plate clamped at both ends and driven by ocean surface wave motion. The analysis revealed that the coupling effects generate both short and long-crested waves along the plate, with the short crested flexural waves being particularly significant for power generation. Wegert et al. (2026) extended the methodology reported by Renzi (2016) by deriving the governing equations in dimensional form, as opposed to non-dimensionalised form. Additionally, this work presented a three-dimensional derivation that accommodates poling angle rotation within the piezoelectric layers, and includes formulations for both surface mounted as well as submerged PWECs. Using piezoelectric bimorphs in wave energy conversion can effectively harness mechanical deformation caused by ocean waves to generate electrical energy. Their design allows for flexibility and adaptability, which enhances durability under varying stress conditions. Despite these advancements, most existing PWECs rely on conventional substrates, which motivates the exploration of auxetic metamaterials in wave energy harvesting.

In recent years, with research interest in mechanical metamaterials, auxetic metamaterials have received significant attention to enhance the efficiency and power output of piezoelectric energy harvesters. Auxetic metamaterials possess the unique ability to expand in the lateral direction upon tensile action in the longitudinal direction, resulting in a negative Poisson's ratio (NPR). Inspired by an ancient Japanese art form, origami has been adopted as a scientific method for developing systems with deployable and dynamic architectures, some of which exhibit auxetic properties (Wang et al., 2026). Various studies have examined the influence of auxetic characteristics on piezoelectric energy harvesters (Roy Chowdhury et al., 2021; Fey et al., 2016; Topolov and Bowen, 2015). Li et al. (2017) introduced a piezoelectric bimorph that uses an auxetic substrate to enhance the energy harvesting of vibrations by increasing the transverse stress in the piezoelectric layers. This innovative design resulted in significantly higher power output, with an average generation 2.76 times higher than traditional bimorphs. Similarly, an auxetic cantilever beam energy harvester excited by a harmonic acceleration of 1 m s^{-2} at 3 Hz was able to produce 2.51 times more power than an equivalent plain cantilever beam energy harvester (Farhangdoust, 2020). The functionally graded (FG) graphene origami-enabled (GOE) auxetic metamaterial is an advanced class of materials that combines the exceptional mechanical properties of graphene origami (GOri) structures with functionally graded design principles (Li and Li, 2025; Yang et al., 2025b). This innovative material exhibits unique auxetic behaviour that significantly improves its energy absorption capacity and overall flexibility (Yang et al., 2025a; Nguyen and Nguyen, 2026). Recent advances in fabrication techniques and computational modelling have optimised the mechanical performance of FG-GOEAMs. As a result, these materials are increasingly being explored for diverse applications in the aerospace (X. Zhang et al., 2026; Le et al., 2026; Chi Hai et al., 2026), automotive (Vu and Tran, 2025) and structural engineering (Liu et al., 2026) sectors. For example, a composite aerogel-based metamaterial with excellent mechanical, electromagnetic, and thermal properties was developed with extensive applications in the aerospace sector (X. Zhang et al., 2026). A piezoelectric energy harvester with an FG-GOEAM core was developed to determine the power output enhancement relative to conventional harvesters. The study found that the GOri architecture facilitates significant vibrational tuneability and improves electromechanical coupling (Ebrahimi and Parsi, 2026b). Ebrahimi and Parsi (2026a) developed a bimorph energy harvester constructed from PZT-5H piezoelectric layers and an FG-GOEAM substrate. By optimising the graphene content and the degree of origami folding, the bimorph achieves tuneable resonant frequencies, significantly improving electromechanical performance, notably a 14% increase in output power compared to traditional copper (Cu)-based harvesters. The FG auxetic structure enables controlled modification of stiffness and strain distribution, which can lead to improved electromechanical coupling and enhanced energy absorption (Krishnaswamy et al., 2020). Additionally, Ren et al. (2026) discusses the adjustment of material deposition to tune performance of a photothermal superhydrophobic metamaterial. Despite these developments, research into piezoelectric energy harvesters with auxetic cores is still in its nascent stage.

Contribution of this work to the field: In contrast to existing studies related to PWECs that consider conventional substrates or surface-mounted piezoelectric devices, this work introduces and analyses a PWEC fundamentally re-engineered through the incorporation of an FG-GOEAM as its structural substrate. Specifically, this study presents the first fully coupled hydroelectromechanical formulation of a submerged piezoelectric bimorph plate in which the load-bearing core itself is a functionally graded GOE auxetic metamaterial, thereby embedding NPR behaviour directly into the PWEC architecture. Building upon the hypersingular boundary integral approach proposed by Wegert et al. (2026), the present work extends this methodology to explicitly account for the metamaterial constitutive properties of the FG-GOEAM substrate, obtained via a genetic programming-based material design approach (Murari et al., 2024). This integration explores the influence of auxeticity in PWEC models. By varying GOri content, folding degree and distribution patterns, the substrate properties can potentially be tailored to match specific wave environments, allowing optimisation of performance for different deployment conditions. The auxetic behaviour promotes enhanced deformation under cyclic wave loading, which, as reported (Krishnaswamy et al., 2020), may reduce stress concentrations and improve structural resilience in dynamic marine environments. Additionally, a comprehensive numerical investigation is conducted to examine how the FG-GOEAM-based PWEC responds when employing either lead zirconate titanate (PZT-5H) piezoelectric or polyvinylidene fluoride (PVDF) layers, with particular emphasis on comparative energy absorption performance.

2. Metamaterial and methods

2.1. Auxetic metamaterial-based bimorph plate wave energy converter

In this work, we use the hydroelectromechanical model described in Wegert et al. (2026). Namely, we consider a bimorph plate wave

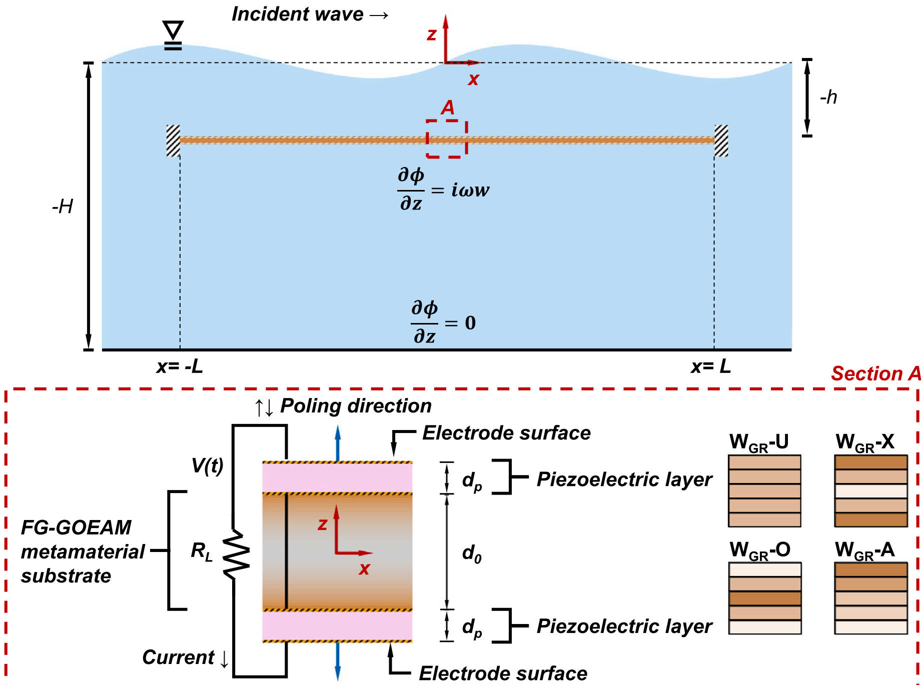

Fig. 1. Schematic showing bimorph–fluid system and a detailed view of the piezoelectric bimorph showing the series configuration between the piezoelectric layers.

energy converter with an auxetic metamaterial substrate located on the xz–plane, as shown in Fig. 1. We assume that the plate is thin and can be modelled using Kirchhoff plate theory. The 2D fluid domain is assigned as $\Omega = (\mathbb{R} \times (-H, 0)) \setminus \Gamma$, where $\Gamma = (-L, L) \times \{-h\}$ denotes the region occupied by the cross section of the bimorph plate. In order to apply linear water wave theory, we assume a viscosity-free, constant-density, incompressible fluid undergoing irrotational flow. This formulation is valid provided the wave amplitude is small compared to the wavelength, but it does not account for nonlinear wave effects, viscous dissipation or wave breaking which come into effect under larger amplitude waves (X. Zhang et al., 2026; Chiang et al., 2005). The plate has a length $2L$ and thickness $d_b = d_0 + 2d_p$. The FG-GOEAM core layer is sandwiched between two piezoelectric layers, as shown in Section A of Fig. 1.

The thickness of the auxetic metamaterial is indicated as d_0, while the thickness of each piezoelectric layer is indicated as d_p. The piezoelectric layers are connected in series with vertical poling as shown in Fig. 1. The resistance R_L is connected to the piezoelectric layers. We assume that all FG layers are perfectly bonded and that the electrodes completely cover each piezoelectric layer. The bimorph plate is immersed in a fluid to a depth h, and the total depth of the fluid is H.

By adopting a harmonic time-dependence $e^{-i\omega t}$ at the angular frequency ω, we can express the model of Wegert et al. (2026) as

$$\begin{aligned}
&\Delta\phi = 0 && (x,z) \in \Omega,\\
&\partial_z\phi = 0 && (x,z) \in \mathbb{R}\times\{H\},\\
&\partial_z\phi = \frac{\omega^2}{g}\phi && (x,z) \in \mathbb{R}\times\{0\},\\
&\partial_z\phi = -\mathrm{i}\omega \mathrm{w} && (x,z) \in \Gamma,\\
&\left[D_{11}^0 + D_{11}^p + \frac{\omega\eta^2}{\omega C + Gi}\right]\partial_x^4 \mathrm{w} - I_0\omega^2 \mathrm{w} = \mathrm{i}\omega\rho_w [\![\phi]\!] && (x,z) \in \Gamma,\\
&[\![\partial_z\phi]\!] = 0 && (x,z) \in \Gamma,\\
&\left\{\partial_x\phi^{sc} \mp \mathrm{i}k\phi^{sc}\right\} \to 0 && x \to \pm\infty,
\end{aligned} \tag{1}$$

with either clamped–clamped boundary conditions:

$$\mathrm{w} = \partial_x \mathrm{w} = 0 \quad \text{for } x = \pm L, \tag{2}$$

or simply supported boundary conditions:

$$\mathrm{w} = \partial_x^2 \mathrm{w} = 0 \quad \text{for } x = \pm L. \tag{3}$$

In the above, ϕ is the velocity potential; $\Delta \equiv \partial_x^2 + \partial_z^2$ is the Laplacian operator for the xz-plane; g is gravity; ρ_w is the density of the fluid; w is the complex-valued plate displacement; D_{11}^0 is the bending rigidity of the substrate; D_{11}^p is the bending rigidity of the piezoelectric layers; $\eta = \frac{1}{2}(d_0 + d_p)\hat{e}_{31}$ is the piezoelectric coupling; $C = \frac{\hat{\kappa}_{33}^{\varepsilon}(\theta)}{2d_p}$ is the electrical surface capacitance; $G = \mathrm{d}R_L/\mathrm{d}A$ denotes the surface conductance; I_0 is the static moment of mass; $[\![\phi]\!]$ indicates the potential jump across the plate, defined as the difference between its upper (ϕ_+) and lower (ϕ_-) values; $\phi^{sc} = \phi - \phi^{in}$ is the scattered wave potential where

$$\phi^{in}(x,z) = \frac{-\mathrm{i}gA}{\omega\cosh kH}\mathrm{e}^{\mathrm{i}kx}\cosh k(z+H), \tag{4}$$

denotes the velocity potential of a plane incident wave with A as the amplitude; and k is the real and positive solution of the dispersion equation

$$k\tanh(kH) = \frac{\omega^2}{g}. \tag{5}$$

In the above $D_{11}^p = 2d_p\left(\frac{d_p^2}{3} + \frac{d_0 d_p}{2} + \frac{d_0^2}{4}\right)Q_{11}^E$, where Q_{11}^E is the stiffness of the piezoelectric layers. For further details regarding the model, we refer the reader to Wegert et al. (2026).

In the next section, we describe how the FG-GOEAM substrate can be incorporated into the model using D_{11}^0 and I_0.

2.2. GOri-enabled auxetic metamaterials

The substrate is comprised of a GOri-reinforced Cu matrix to generate a metallic Cu metamaterial. In order to define the distribution and characterisation of the GOE auxetic metamaterial, we incorporate the formations documented by Zhao et al. (2022). We consider four

GOri dispersions as illustrated in Section A of Fig. 1, namely, uniform (W_{GR}-U), symmetrical (W_{GR}-X, W_{GR}-O) and asymmetrical (W_{GR}-A) distribution patterns, whose mathematical expressions are as follows

$$V_{\mathrm{GR}}(k)=\begin{cases}V_{\mathrm{GR}}, & W_{GR}\text{-U}\\ 2V_{\mathrm{GR}}\frac{|2k-N_L-1|}{N_L}, & W_{GR}\text{-X}\\ 2V_{\mathrm{GR}}\left(1-\frac{|2k-N_L-1|}{N_L}\right), & W_{GR}\text{-O}\\ V_{\mathrm{GR}}\frac{2k-1}{N_L}, & W_{GR}\text{-A}\end{cases} \tag{6}$$

where $V_{GR}(k)$ denotes the volume fraction of GOri in the kth layer ($k = 1, 2, \ldots, N_L$) and N_L is the total number of layers. The total volume fraction of GOri in the plate is derived from the weight fraction as

$$V_{\mathrm{GR}}=\frac{W_{GR}}{W_{GR}+(\rho_{GR}\,/\rho_{Cu}\,)(1-W_{GR})}. \tag{7}$$

Various metamaterial distributions are considered, namely, uniform (H_{GR}-U), symmetrical (H_{GR}-X, H_{GR}-O) and asymmetrical (H_{GR}-A) distribution patterns, whose mathematical expressions are as follows

$$H_{\mathrm{GR}}(k)=\begin{cases}H_{\mathrm{GR}}, & H_{GR}\text{-U}\\ H_{\mathrm{GR}}\cos(\frac{\pi z}{d_0}), & H_{GR}\text{-X}\\ H_{\mathrm{GR}}(1-\cos(\frac{\pi z}{d_0})), & H_{GR}\text{-O}\\ H_{\mathrm{GR}}\cos(\frac{\pi z}{2d_0}+\frac{\pi}{4}), & H_{GR}\text{-A}\end{cases} \tag{8}$$

where H_{GR} is the GOri folding degree quantified as the hydrogen (H) coverage (0%–100%). H_{GR} = 0% denotes pristine graphene without any folding, while higher H_{GR} implies more GOri folding. We incorporate the genetic programming (GP)-assisted micromechanics models developed by Zhao et al. (2022). The GP method improves the traditional Halpin–Tsai micromechanics model to determine the effective elastic modulus (E_C) by incorporating modification functions $f_{(E,\rho,\upsilon,\alpha)}(H_{GR}, V_{GR}, T)$ that account for H coverage (H_{GR}), GOri volume fraction (V_{GR}) and temperature (T). In addition, enhancements are made to the Rule-of-Mixtures to determine the effective Poisson's ratio (ν_c), density(ρ_c) and thermal expansion coefficient (α_c) as

$$E_c=\frac{1+\xi_{GR}\eta_{GR}V_{\mathrm{GR}}}{1-\eta_{GR}V_{\mathrm{GR}}}E_{\mathrm{Cu}}\times f_E(H_{\mathrm{GR}},V_{\mathrm{GR}},T), \tag{9a}$$

$$\rho_c=(\rho_{\mathrm{GR}}V_{\mathrm{GR}}+\rho_{\mathrm{Cu}}V_{\mathrm{Cu}})\times f_\rho(V_{\mathrm{GR}},T), \tag{9b}$$

$$\upsilon_c=(\upsilon_{\mathrm{GR}}V_{\mathrm{GR}}+\upsilon_{\mathrm{Cu}}V_{\mathrm{Cu}})\times f_\upsilon(H_{\mathrm{GR}},V_{\mathrm{GR}},T), \tag{9c}$$

$$\alpha_c=(\alpha_{\mathrm{GR}}V_{\mathrm{GR}}+\alpha_{\mathrm{Cu}}V_{\mathrm{Cu}})\times f_\alpha(V_{\mathrm{GR}},T), \tag{9d}$$

where material (η_{GR}) and size (ξ_{GR}) coefficients are denoted, using the length l_{GR} and thickness t_{GR} of graphene as

$$\eta_{GR}=\frac{E_{GR}/E_{Cu}-1}{E_{GR}/E_{Cu}+\xi_{GR}}, \tag{10a}$$

$$\xi_{GR}=2\frac{l_{GR}}{t_{GR}}. \tag{10b}$$

The modification functions are given by

$$\begin{aligned}f_E\ &=1.11-1.22V_{\mathrm{GR}}-0.134(T/T_0)+0.559V_{\mathrm{GR}}(T/T_0)\\ &-5.5H_{\mathrm{GR}}V_{\mathrm{GR}}+38H_{\mathrm{GR}}(V_{\mathrm{GR}})^2-20.6(H_{\mathrm{GR}}V_{\mathrm{GR}})^2,\end{aligned} \tag{11a}$$

$$f_\rho=1.01-0.0131(T/T_0)-2.01(V_{\mathrm{GR}})^2, \tag{11b}$$

$$\begin{aligned}f_\nu\ &=1.01-1.43V_{\mathrm{GR}}+0.165(T/T_0)-16.8H_{\mathrm{GR}}V_{\mathrm{GR}}\\ &-1.1H_{\mathrm{GR}}V_{\mathrm{GR}}(T/T_0)+16(H_{\mathrm{GR}}V_{\mathrm{GR}})^2,\end{aligned} \tag{11c}$$

$$f_\alpha=0.794-16.8(V_{\mathrm{GR}})^2-0.0279(T/T_0)^2+0.182(T/T_0)(1+V_{\mathrm{GR}}). \tag{11d}$$

The functionally graded GOE auxetic metamaterial substrate exhibits pronounced NPR characteristics, motivating a parametric investigation of GOri folding degree and metamaterial distribution patterns.

As shown in Fig. 2(a), low H coverage in the GOri reinforcement reduces the Poisson's ratio of the GOri/Cu layers. Increasing H coverage promotes the transition from a GOri/Cu layer to a GOE auxetic metamaterial, resulting in a reduction in Young's modulus. The effect of metamaterial distribution is shown in Fig. 2(b). The H_{GR}-X and H_{GR}-O metamaterial distribution patterns are symmetric, with auxetic behaviour concentrated in the internal layers and edge layers, respectively, whereas the H_{GR}-U distribution exhibits auxetic behaviour across all layers. Figs. 2(c) and (d) depict the influence of GOri weight fraction and GOri distribution on the Poisson's ratio and Young's modulus of the FG-GOEAM substrate, respectively. Increasing GOri content induces auxetic behaviour within the FG layers and increases Young's modulus, with W_{GR} = 2.5% resulting in the largest NPR magnitudes. For the W_{GR}-X distribution, auxetic behaviour is dominant in the edge layers, whereas the internal layers exhibit positive Poisson's ratio. In contrast, the W_{GR}-O distribution exhibits NPR values in the internal layers and positive Poisson's ratios near the surfaces.

To incorporate the FG-GOEAM substrate into the hydroelectromechanical model in Section 2.1 we define the plane-stress reduced stiffness (Murari et al., 2023) of the FG-GOEAM substrate as

$$Q_{11}^0=\frac{E_c}{1-\nu_c^2}, \tag{12}$$

where E_c and ν_c are the effective elastic modulus and Poisson's ratio of the functionally graded GOE auxetic metamaterial, respectively. From the law of elasticity (Reddy, 2003), the normal stress σ_{11} is obtained as

$$\sigma_{11}=Q_{11}^0\varepsilon_{11}, \tag{13a}$$

where strain ε_{11} is given by

$$\varepsilon_{11}=-z\partial_x^2\mathrm{w}. \tag{13b}$$

The dimensional bending stiffness D_{11}^0, dimensionless bending stiffness d_{11}^0 and inertia I_0 are given by

$$D_{11}^0=\int_{-d_0/2}^{d_0/2}Q_{11}^0z^2\,\mathrm{d}z, \tag{14a}$$

$$d_{11}^0=\frac{D_{11}^0(1-\nu_{Cu}^2)}{E_{Cu}d_0^3}, \tag{14b}$$

and

$$I_0=\int_{-d_0/2}^{d_0/2}\rho_c\,\mathrm{d}z+2\int_{d_0/2}^{d_0/2+d_p}\rho_p\,\mathrm{d}z, \tag{15}$$

where ρ_c is the density of the functionally graded GOE auxetic metamaterial as determined from Eq. (9b) and ρ_p is the density of the piezoelectric material. Eqs. (15) and (14a) can then be inserted into the model given in Eq. (1). The novelty of the present study lies in the introduction of an FG auxetic metamaterial substrate, which leads to modified bending stiffness (d_{11}^0) and inertia (I_0) parameters that are not described in existing formulations such as Wegert et al. (2026).

Unlike the assumption of a homogeneous and isotropic silicone substrate as considered by Wegert et al. (2026), the present work considers a through-thickness variation of material properties governed by the GOri volume fraction. This introduces layer-wise variations in Poisson's ratio, density and thermo-mechanical properties, as shown in Eqs. (6)–(9), which in turn modify the global structural response.

From a modelling perspective, the study integrates molecular dynamics and GP-informed modification functions into the modified Halpin–Tsai and rule-of-mixtures models (Zhao et al., 2022), thus enabling accurate prediction of FG auxetic metamaterial behaviour. These relations culminate in modified expressions for the reduced stiffness (Eq. (12)) and normal stress (Eq. (13a)), from which the revised stiffness and inertia terms are derived. Importantly, the FG layout introduces a tuneable structural response, allowing controlled tuning of the dynamic behaviour of the PWECs, which is not attainable with uniform substrates.

The influence of auxetic material properties on the dimensionless bending d_{11}^0 response is displayed in Fig. 3. The influence of H_{GR} and W_{GR} with various GOri distribution patterns on the bending stiffness of an FG-GOEAM plate is shown in Fig. 3. The uniform metamaterial distribution pattern is used for illustration as NPR properties are

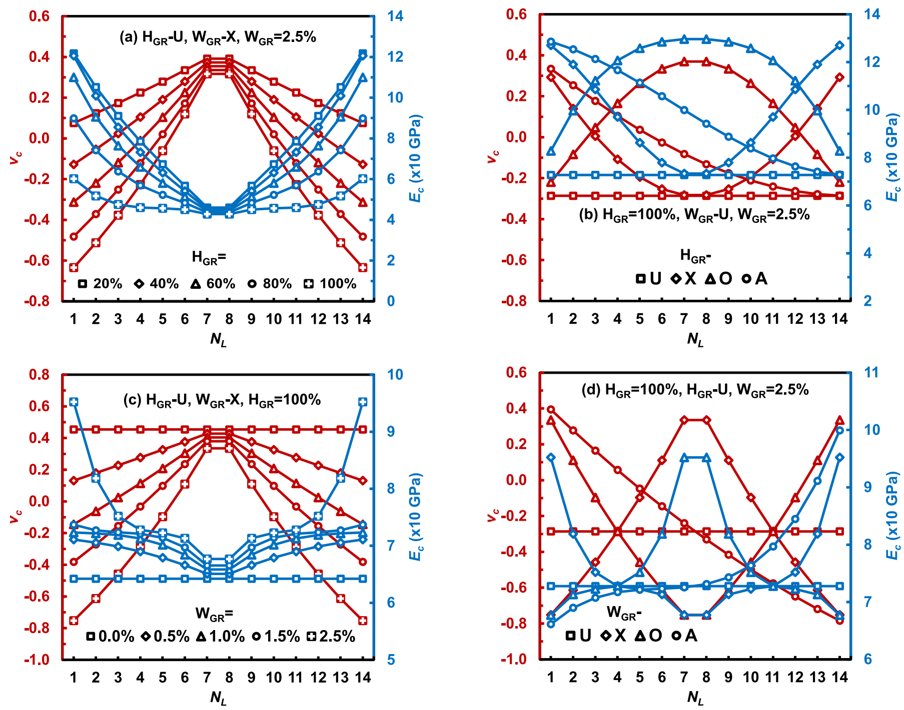

Fig. 2. Layer-wise variation of the Young's modulus and Poisson's ratio of the functionally graded GOE auxetic substrate based on (a) GOri folding degree, (b) metamaterial distribution patterns, (c) GOri content and (d) GOri distribution patterns, as determined by Eqs. (9a) and (9c).

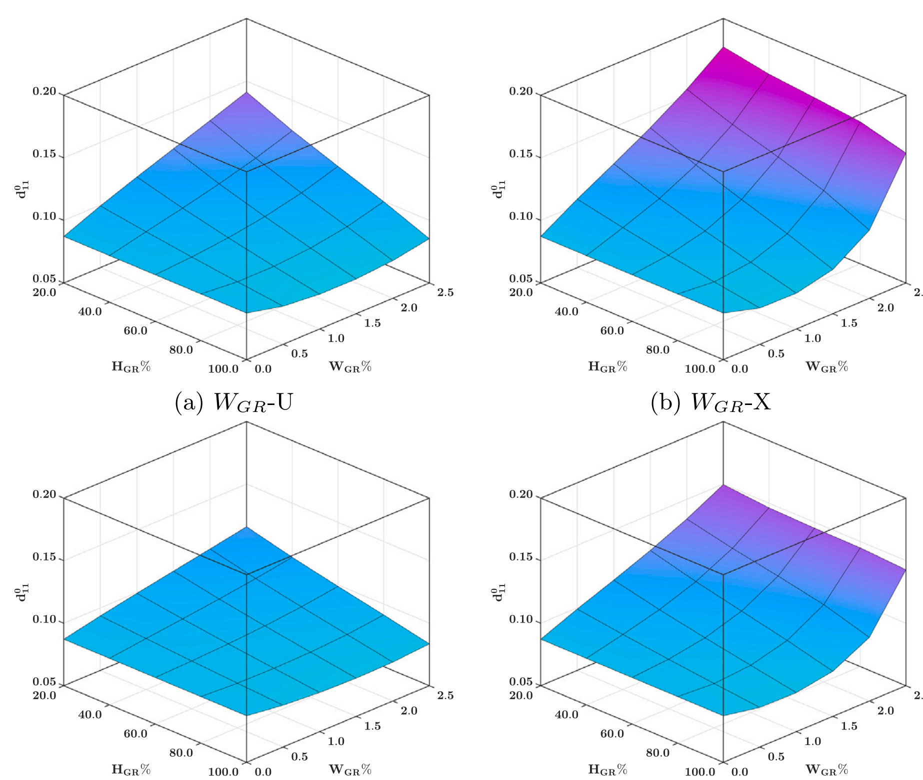

(a) W_{GR}-U (b) W_{GR}-X (c) W_{GR}-O (d) W_{GR}-A

Fig. 3. Effect of the H coverage and GOri content on the dimensionless bending stiffness of an FG-GOEAM substrate with uniform metamaterial distribution H_{GR}-U and various GOri distribution patterns, as determined from Eq. (14b).

exhibited in all the layers as shown in Fig. 2(b). It can be observed that a low GOri content ($W_{GR} \leq 1.0\%$) reduces the bending stiffness of the substrate due to the reduction in the Poisson's ratio magnitude. However, an adequate GOri ($W_{GR} > 1.0\%$) increases the bending stiffness due to the transformation of the composite (GOri/Cu) to a GOE auxetic metamaterial which possesses high NPR characteristics. Increasing the H coverage leads to a gradual reduction in the bending stiffness, owing to the formation of the GOE auxetic metamaterials. The W_{GR}-X distribution pattern results in the highest bending stiffness due to the GOri reinforcement in the surface layers.

2.3. Solution method

The model given in Eq. (1) is solved using the approach described in Wegert et al. (2026). Specifically, we employ a modal expansion method (Newman, 1994) to reduce the diffraction and radiation problems to hypersingular integral equations governing the wave–structure interaction, which are then solved by a constant panel method. This approach represents continuous structural deformation as a finite linear combination of orthogonal mode shapes. By transforming the partial differential equations into discrete sets of modal coordinates, the method significantly reduces computational costs while maintaining high fidelity in depicting the wave–structure interaction between the incident wave field and the PWEC. The plate domain is discretised into finite panels with midpoint collocation, enabling stable and accurate evaluation of the diffraction potential for submerged configurations. The numerical model accommodates both simply supported and clamped boundary conditions, as well as variations in material properties.

The dynamic response of the piezoelectric bimorph is obtained via a dry-mode expansion approach where the displacement and velocity potential are expressed in terms of truncated modal series. The coupled system of equations is assembled into a matrix form, incorporating structural stiffness, mass, added mass and hydrodynamic damping effects, and solved for the modal coefficients. The method's convergence and validity has been verified by comparison with an eigenfunction matching method (Wegert et al., 2026).

Material parameters are derived from established literature sources, including GP-assisted micromechanics models (Zhao et al., 2022; Murari et al., 2024) for the FG-GOE auxetic metamaterial substrate Eqs. (9)–(11) and standard constitutive data for piezoelectric materials (Table 2). The analysis follows a structured computational procedure: (i) evaluation of the layer-wise material properties across the N_L FG layers, (ii) computation of effective stiffness and inertia parameters via Eqs. (15) and (14a), respectively, (iii) solution of the coupled structural and hydrodynamic systems using boundary integral and modal methods, and (iv) determine reflection, transmission and energy absorption coefficients. This structured workflow ensures numerical stability, physical consistency as well as full reproducibility of the results.

2.4. Reflection and transmission

In analysing wave interactions with the piezoelectric bimorph plates, we define two key coefficients: reflection (R) and transmission (T). These coefficients quantify how much wave energy is reflected by the PWEC versus how much advances beyond the PWEC. These relationships are essential in determining the efficiency of the PWEC. The reflection and transmission coefficients are defined so that, asymptotically,

$$\phi(x,z) \sim \begin{cases} -\frac{\mathrm{i}gA}{\omega\cosh kH}\cosh(k(z+H))(\mathrm{e}^{\mathrm{i}kx}+R\mathrm{e}^{-\mathrm{i}kx}) & \text{as } x\to-\infty, \\ -\frac{\mathrm{i}gA}{\omega\cosh kH}\cosh(k(z+H))T\mathrm{e}^{\mathrm{i}kx} & \text{as } x\to+\infty. \end{cases} \tag{16}$$

Using these, the proportion of energy absorbed at a given frequency can be calculated as

$$1-|R|^2-|T|^2. \tag{17}$$

Table 1
Room temperature material properties of pristine Cu and graphene.

Properties	Pristine Cu Matrix	Graphene
Young's modulus	65.79 GPa	0.9296 TPa
Poisson's ratio	0.387	0.220
Mass density	8.80 g/cm^3	1.80 g/cm^3
Thermal expansion coefficient	16.51×10^{-6} K^{-1}	-3.98×10^{-6} K^{-1}

Table 2
Piezoelectric material values for PVDF and PZT-5H with a vertical poling direction.

Properties	PVDF (Kepler, 1995)	PZT-5H (Yang, 2005)
Q^E_{11} (GPa)	3.54	65.5
κ^ε_{33} (Fm^{-1})	1.13×10^{-10}	1.77×10^{-8}
e_{31} (Cm^{-2})	0.113	−23.2
ρ	1780	7500

2.5. Efficiency in irregular ocean states

To measure the energy absorption efficiency, we employ the methodology proposed by Wegert et al. (2026). Namely, we adopt the Pierson–Moskowitz spectrum (Pierson and Moskowitz, 1964; Dean and Dalrymple, 1991). For an ocean state with peak period T_p, the spectral energy distribution is frequency-dependent. The corresponding absorption efficiency follows

$$E_{\mathrm{eff}} = \frac{\int_0^\infty S(\omega)\left(1-|R|^2-|T|^2\right)\,\mathrm{d}\omega}{\int_0^\infty S(\omega)\,\mathrm{d}\omega}, \tag{18}$$

where $S(\omega)$ is given by the Pierson–Moskowitz spectrum

$$S(\omega) = ag^2\omega^{-5}\exp\left(-\frac{5}{4}\left(\frac{2\pi}{T_p\omega}\right)^4\right), \tag{19}$$

with $a = 8.1\times10^{-3}$.

3. Results and discussion

The FG-GOEAM substrate is constructed from Cu matrix reinforced with GOri filler. The material properties of pristine Cu matrix and graphene are shown in Table 1.

The substrate has a thickness $d_0 = 0.01$ m and the total number of layers $N_L = 14$. The geometric properties of the pristine graphene are $l_{GR} = 83.76$ Åand $t_{GR} = 3.4$ Ådenoting the length and thickness, respectively. Unless otherwise stated, the properties that pertain to this study are as follows: clamped–clamped boundary conditions, full submersion at $h = 2$ m, $G/C = 1$ s^{-1}, uniform metamaterial distribution H_{GR}-U, symmetric GOri distribution W_{GR}-X, H coverage $H_{GR} = 100\%$ and GOri content $W_{GR} = 2.5\%$. PZT-5H piezoelectric layers are considered for the current study due to their high energy absorption properties as a result of their high piezoelectric coupling coefficient as given in Table 2.

Furthermore, the piezoelectric material tensors for PZT-5H with a vertical poling direction are

$$S^E(\theta=0^\circ) = \begin{pmatrix} 16.7 & -4.84 & -8.5 & 0 & 0 & 0 \\ -4.84 & 16.7 & -8.5 & 0 & 0 & 0 \\ -8.5 & -8.5 & 20.8 & 0 & 0 & 0 \\ 0 & 0 & 0 & 43.5 & 0 & 0 \\ 0 & 0 & 0 & 0 & 43.5 & 0 \\ 0 & 0 & 0 & 0 & 0 & 42.9 \end{pmatrix} \times 10^{12}\,(\mathrm{m^2N^{-1}}), \tag{20a}$$

$$d(\theta=0^\circ) = \begin{pmatrix} 0 & 0 & 0 & 0 & 7.39 & 0 \\ 0 & 0 & 0 & 7.39 & 0 & 0 \\ -2.75 & -2.75 & 5.94 & 0 & 0 & 0 \end{pmatrix} \times 10^{10}\,(\mathrm{mV^{-1}}), \tag{20b}$$

$$\kappa^\sigma(\theta=0^\circ) = \begin{pmatrix} 2.76 & 0 & 0 \\ 0 & 2.76 & 0 \\ 0 & 0 & 3.04 \end{pmatrix} \times 10^{-8}\,\mathrm{Fm^{-1}}. \tag{20c}$$

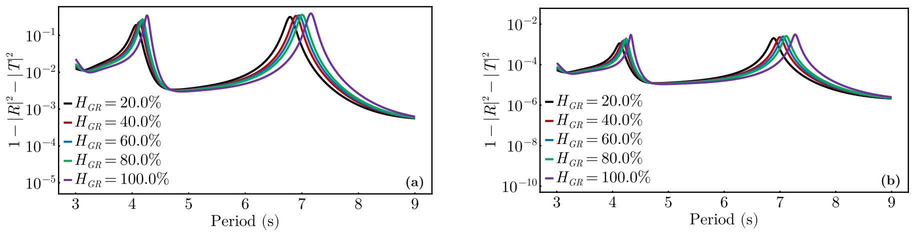

Fig. 4. Effect of H coverage on the energy absorption of a piezoelectric FG-GOEAM bimorph with (a) PZT-5H and (b) PVDF.

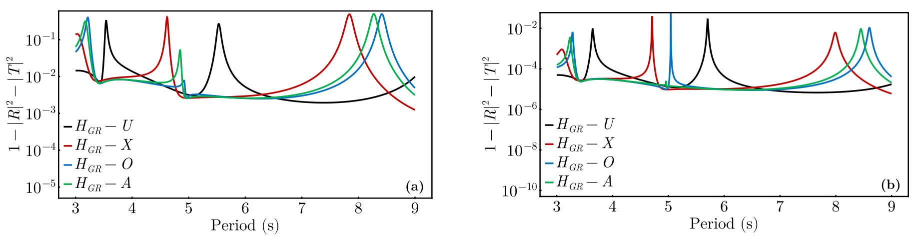

Fig. 5. Effect of the metamaterial distribution pattern on the energy absorption of a piezoelectric FG-GOEAM bimorph with (a) PZT-5H and (b)PVDF (with W_{GR}-U).

Table 3
Effect of H coverage on the energy absorption efficiency of piezoelectric FG-GOEAM bimorphs.

H_{GR}	PZT-5H (%)	PVDF (%)
20%	2.647	0.01145
40%	2.677	0.01185
60%	2.689	0.01207
80%	2.698	0.01232
100%	2.699	0.01308

Table 4
Effect of the metamaterial distribution on the energy absorption efficiency of piezoelectric FG-GOEAM bimorphs.

Metamaterial distribution	PZT-5H (%)	PVDF (%)
H_{GR}-U	2.056	0.03290
H_{GR}-X	1.997	0.01919
H_{GR}-O	1.544	0.04907
H_{GR}-A	1.579	0.00764

Table 5
Effect of the GOri content on the energy absorption efficiency of piezoelectric FG-GOEAM bimorphs.

W_{GR}	PZT-5H (%)	PVDF (%)
Pristine Cu	1.809	0.03241
0.5%	3.187	0.03448
1.0%	3.237	0.03457
1.5%	2.040	0.03284
2.5%	2.699	0.01308

Fig. 4 and Table 3 illustrate the energy absorption and efficiency of piezoelectric FG-GOEAM bimorphs over a 5s period, respectively. The bimorph with H_{GR} = 100% exhibits higher energy absorption compared to H_{GR} = 20%, indicating that increasing H coverage promotes energy harvesting performance for both PZT-5H and PVDF configurations. This behaviour arises primarily from the reduction in bending stiffness associated with increases in H coverage, as demonstrated in Fig. 3(b). As shown in Fig. 2(a), higher H coverage produces lower effective Young's moduli within FG layers, resulting in a more flexible substrate. This reduced stiffness enhances flexural deformation under wave excitation, leading to increased curvature of the bimorph. The enhanced curvature increases the longitudinal strain exhibited by the piezoelectric layers. As a result, the charge generation is improved through the piezoelectric effect. Furthermore, the auxetic nature of the GOE auxetic metamaterial substrate facilitates lateral expansion under flexural loading, thereby enhancing the strain transfer to the piezoelectric layers. Conversely, stiffer substrates inhibit flexural deformation and strain transfer, resulting in weaker electromechanical coupling and reduced energy absorption. Consequently, increasing the H coverage enhances energy harvesting by promoting more flexible, auxetic-driven deformation, which can facilitate strain transfer and improve the piezoelectric response.

The effect of the metamaterial distribution patterns on the energy absorption of piezoelectric FG-GOEAM bimorphs with PZT-5H and PVDF layers is shown in Figs. 5(a) and (b), respectively. For bimorphs incorporating PZT-5H, the FG-GOEAM bimorph with the H_{GR}-U metamaterial distribution exhibits the highest energy absorption among all considered patterns. In contrast, for bimorphs incorporating PVDF layers, the H_{GR}-O distribution yields the highest energy absorption efficiency, as reported in Table 4. This behaviour indicates that the optimal metamaterial distribution depends on the mechanical characteristics of the piezoelectric layer and its capacity for electromechanical coupling. In the PZT-5H case, the fully auxetic distribution reduces the effective stiffness (Fig. 2(b)) and bending rigidity (Fig. 3(b)), thereby promoting larger flexural deformation under wave loading. The resulting increase in curvature enhances strain transfer to the piezoelectric layers, leading to stronger electromechanical coupling and increased energy absorption. For the more flexible PVDF-based bimorphs, the symmetrical H_{GR}-O distribution provides a more favourable through-thickness strain distribution by reducing excessive strain concentration while maintaining sufficient global deformation. This leads to a more uniform strain field within the piezoelectric layers, improving charge generation efficiency and resulting in higher overall energy absorption efficiency in piezoelectric FG-GOEAM bimorphs.

The influence of the GOri content on the energy absorption and efficiency of piezoelectric FG-GOEAM bimorphs is illustrated in Fig. 6 and Table 5, respectively. For $W_{GR} \leq 1.0\%$, increasing the GOri content leads to higher energy absorption. This is primarily attributed to a reduction in Poisson's ratio towards lower positive values (Fig. 2(c)), which reduces the effective stiffness and flexural rigidity of the substrate (Fig. 3(b)). The resulting increase in structural compliance promotes greater flexural deformation under wave loading, leading

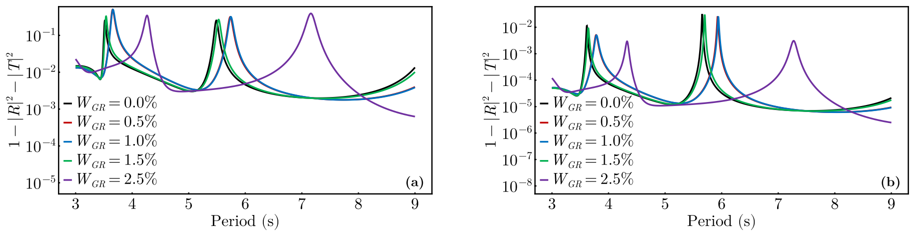

Fig. 6. Effect of the GOri content on the energy absorption of a piezoelectric FG-GOEAM bimorph with (a) PZT-5H and (b) PVDF.

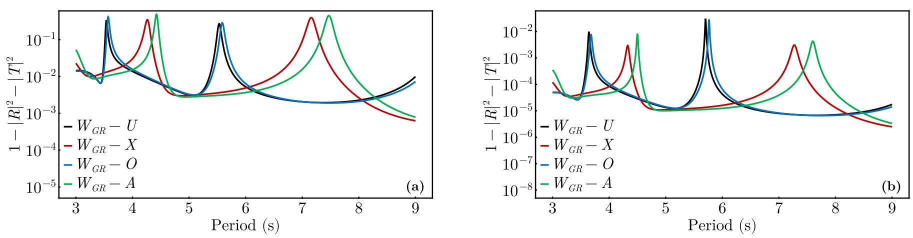

Fig. 7. Effect of GOri distribution pattern on the energy absorption of a piezoelectric FG-GOEAM bimorph with (a) PZT-5H and (b) PVDF.

Table 6
Effect of GOri distribution pattern on the energy absorption efficiency of piezoelectric FG-GOEAM bimorphs.

Graphene distribution	PZT-5H (%)	PVDF (%)
W_{GR}-U	2.056	0.03290
W_{GR}-X	2.699	0.01308
W_{GR}-O	2.378	0.03340
W_{GR}-A	2.518	0.01514

Table 7
Effect of the edge boundary conditions and piezoelectric material selection on the energy absorption efficiency of piezoelectric FG-GOEAM bimorphs.

Boundary condition	PZT-5H (%)	PVDF (%)
Simply supported	1.260	0.01072
Clamped	2.699	0.01308

to enhanced curvature and increased strain transfer to the piezoelectric layers, thereby improving electromechanical coupling and energy output. However, for higher GOri content ($W_{\mathrm{GR}} > 1.0\%$), further increases result in higher Young's modulus and Poisson's ratio, leading to increased effective stiffness and reduced energy absorption. This behaviour is associated with the transition of the GOri/Cu composite into a GOE auxetic metamaterial exhibiting high NPR characteristics. While NPR enhances lateral deformation, the increase in stiffness dominates the structural response, restricting overall flexural deformation and limiting strain transfer in the piezoelectric layers. Despite this reduction in energy absorption at higher GOri content, the FG-GOEAM substrate outperforms the pristine Cu substrate due to its tuneable mechanical properties, which enable enhanced control over deformation and electromechanical coupling.

Figs. 7(a) and (b) depict the influence of the GOri distribution pattern on the energy absorption of piezoelectric FG-GOEAM bimorphs with PZT-5H and PVDF layers, respectively. The corresponding energy absorption efficiencies are summarised in Table 6. The results indicate that the energy absorption depends strongly on the piezoelectric layer material. For the PZT-5H-based bimorph, the symmetrical W_{GR}-X GOri distribution, in which most of the GOri reinforcement is concentrated in the surface layers (Fig. 2(d)), produces the highest energy absorption, followed by the asymmetrical W_{GR}-A distribution. In contrast, for the PVDF-based bimorph, the symmetrical W_{GR}-O distribution, with a larger fraction of GOri located in the internal layers, yields the highest energy absorption, followed by the uniform W_{GR}-U configuration. This behaviour suggests that the optimal GOri distribution is governed by the interaction between the through-thickness strain distribution of the FG-GOEAM substrate and the mechanical compliance of the piezoelectric layer. For the PZT-5H case, which exhibits relatively high stiffness, energy harvesting is enhanced by surface-reinforced bending, where larger strains are concentrated near the outer layers of the bimorph. This enhances stress transfer and increases electromechanical coupling within the piezoelectric layers, resulting in higher energy absorption for FG-GOEAM bimorphs. In contrast, for more flexible PVDF-based bimorphs, distributions that promote a more uniform strain field across the thickness tend to be more effective. The symmetrical W_{GR}-O distribution reduces excessive strain concentration while maintaining sufficient global deformation, thereby improving charge generation efficiency and overall energy absorption efficiency in piezoelectric FG-GOEAM bimorphs.

The material properties of PZT-5H and PVDF are listed in Table 2. As shown in Fig. 8(a) and Table 7, FG-GOE auxetic metamaterial bimorphs incorporating PZT-5H exhibit higher energy absorption and efficiency compared to those with PVDF. This behaviour is attributed to the higher piezoelectric coupling coefficients of PZT-5H, which enable more effective conversion of mechanical strain into electrical charge. Additionally, fully clamped boundary conditions result in marginally higher energy absorption compared to simply supported configurations. This behaviour is attributed to enhanced excitation of the flexural modes under wave-induced loading. Fixed boundary conditions increase the structural stiffness and shift the fundamental frequencies, leading to higher bending strains within the interior region of the bimorph for a given wave input. Thereby enhancing electromechanical coupling in the piezoelectric layers and improving energy conversion efficiency.

The effect of submergence depth on energy absorption and efficiency is illustrated in Fig. 8(b) and Table 8, respectively. The highest energy absorption occurs near the free surface, where wave energy is concentrated. As the submergence depth increases, the available wave-induced excitation decreases due to attenuation of the fluid motion with depth, resulting in reduced structural response of the bimorph. Furthermore, increased depth enhances hydrodynamic added mass and

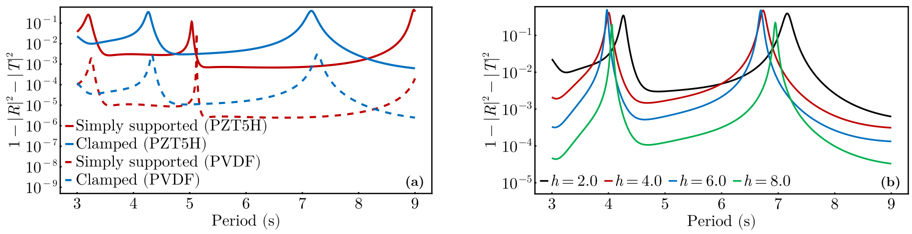

Fig. 8. Effect of (a) piezoelectric material and boundary conditions and (b) submergence depth on the energy absorption of a piezoelectric FG-GOEAM bimorph.

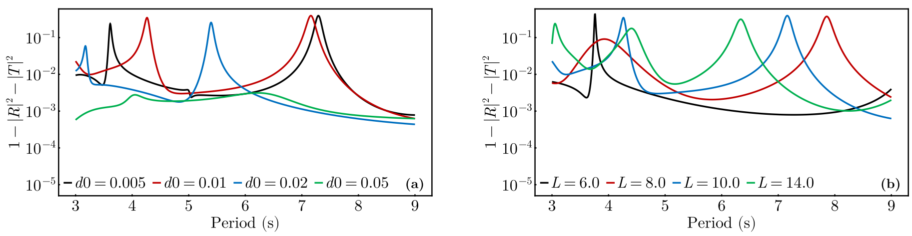

Fig. 9. Effect of (a) substrate thickness d_0 and (b) half-plate length L on the energy absorption of a piezoelectric FG-GOEAM bimorph.

Table 8
Effect of submersion depth on the energy absorption efficiency of piezoelectric FG-GOEAM bimorphs.

h [m]	Efficiency (%)
2	2.699
4	2.442
6	1.495
8	0.3899

Table 9
Effect of substrate thickness d_0 on the energy absorption efficiency of piezoelectric FG-GOEAM bimorphs.

d_0 [m]	Efficiency (%)
0.005	1.154
0.01	2.699
0.02	1.320
0.05	0.1956

Table 10
Effect of half-plate length L on the energy absorption efficiency of piezoelectric FG-GOEAM bimorphs.

L [m]	Efficiency (%)
6	0.9541
8	2.496
10	2.699
14	4.840

radiation damping effects, which alter the system dynamics and reduce the amplitude of vibration. Consequently, energy absorption and conversion efficiency decrease with increasing submergence depth.

The influence of the substrate thickness on the energy absorption and efficiency of the FG-GOE auxetic metamaterial bimorph is shown in Fig. 9(a) and Table 9. The results indicate an optimal thickness ($d_0 \approx 0.01m$) that maximises energy absorption. For small thicknesses, increasing d_0 leads to higher efficiency due to enhanced structural stiffness, which improves stress transfer and electromechanical coupling in the piezoelectric layers. However, further increases in thickness result in a significant reduction in energy absorption. This behaviour is attributed to excessive stiffening of the substrate, which suppresses flexural deformation under wave excitation and limits strain development within the piezoelectric layers (Mutsuda et al., 2019). As a result, the energy conversion efficiency decreases as the structure becomes too rigid to effectively respond to incident wave loading.

The effect of plate length ($2L$) on the energy absorption and efficiency of the auxetic bimorph is summarised in Fig. 9(b) and Table 10, respectively. The results show an increase in the energy absorption with increasing plate length. For shorter plates, the energy absorption is limited due to reduced interaction with the incident wave field and lower flexural deformation. This could have been predicted from intuition because as the plate length increases, a larger section of the wavelength is intercepted, and the structure undergoes greater flexural deformation under wave excitation (Z. Zhang et al., 2026; X. Xie et al., 2014; Vipin and Koley, 2022; Xia et al., 2025). This leads to enhanced curvature and increased strain transfer to the piezoelectric layers, thereby improving electromechanical coupling and energy conversion efficiency in FG-GOE auxetic metamaterial bimorphs. Additionally, longer plates support a wider range of bending modes, which can contribute to stronger resonant interaction with the incoming waves, further enhancing energy absorption.

4. Conclusions

As the demand for clean and sustainable energy continues to grow, ocean wave energy offers a viable yet largely underexploited resource for renewable power generation. The auxetic substrate leverages graphene-based reinforcements and FG architectures, which are becoming feasible through modern fabrication techniques such as layer-wise manufacturing and advanced composite processing. In this study, a comprehensive theoretical model has been used to investigate wave energy conversion using submerged piezoelectric bimorph plates incorporating FG-GOEAM substrates. The model couples plate dynamics, piezoelectric electromechanical behaviour, fluid–structure interaction and electromechanical coupling, and is solved using the method of Wegert et al. (2026).

The following key findings are concluded from the numerical results:

1. Increasing the GOri folding degree enhances energy harvesting by reducing the effective bending stiffness of the substrate and enabling larger flexural deformations.
2. The GOri content exhibits an optimal range, whereby moderate reinforcement promotes auxetic behaviour and improves electromechanical coupling, while excessive GOri content increases stiffness and reduces energy absorption due to the transition to a stiffer GOE auxetic metamaterial response.
3. Metamaterial and GOri distribution patterns that reduce surface-layer stiffness yield higher energy absorption in piezoelectric FG-GOEAM bimorphs, thus highlighting the importance of tuneable strain concentration and flexible surface regions under wave-induced bending.
4. In accordance with the findings of Wegert et al. (2026), bimorphs that incorporate PZT-5H layers outperform PVDF based configurations due to their higher piezoelectric coupling coefficients. Fully clamped boundary conditions provide modest performance improvements compared to simply supported configurations by increasing bending strains near the ends.
5. Compared to a silicone rubber substrate (Renzi, 2016; Wegert et al., 2026), which exhibits greater flexibility and higher energy absorption due to its lower stiffness, the FG-GOEAM substrate provides enhanced structural reinforcement of the PWEC. Although stiffer and absorbs less energy intrinsically, FG-GOEAM maintains effective energy harvesting while improving mechanical robustness, making it a potential material for deployment in ocean and sea environments. Unlike conventional silicone substrates, FG-GOEAM provides expanded parameter control to tune the dynamic response and enhance the efficiency of energy harvesters.

Overall, the results demonstrate the potential of FG-GOE auxetic metamaterial substrates for tailoring the dynamic response and electromechanical performance of PWECs. These findings provide insight into the role of auxetic behaviour and functionally graded materials in wave energy harvesting and establish a foundation for future experimental validation and practical implementation.

CRediT authorship contribution statement

Bill Murari: Writing – original draft, Validation, Methodology, Investigation, Formal analysis, Conceptualization. **Zachary J. Wegert:** Writing – review & editing, Methodology, Formal analysis. **Ben Wilks:** Writing – review & editing, Methodology, Formal analysis, Conceptualization. **Mergen H. Ghayesh:** Writing – review & editing, Supervision. **Ngamta Thamwattana:** Writing – review & editing, Supervision, Formal analysis. **Vivien J. Challis:** Writing – review & editing, Supervision, Formal analysis. **Michael H. Meylan:** Writing – review & editing, Supervision, Formal analysis.

Declaration of competing interest

The authors declare that they have no known competing financial interests or personal relationships that could have appeared to influence the work reported in this paper.

Acknowledgment

This research is supported by the Australian Government through the Australian Research Council (ARC), Discovery Grant DP240102104.

Data availability

Data will be made available on reasonable request.

References

Cai, W., Roussinova, V., Stoilov, V., 2022. Piezoelectric wave energy harvester. Renew. Energy 196, 973–982. http://dx.doi.org/10.1016/j.renene.2022.07.051.

Chen, Y., Wu, M., Tian, Y., Zhang, R., Zhao, W., Du, H., Zhang, C., Du, Y., Du, T., Yuan, H., Si, J., Xu, M., 2026. Recent advances in piezoelectric and triboelectric nanogenerators for ocean current energy harvesting. J. Mar. Sci. Eng. 14 (3), 249. http://dx.doi.org/10.3390/jmse14030249.

Chi Hai, N.L., Hoang, N.T., Huong Binh, N.V., 2026. Dynamic response analysis of FG-GOEAM plates resting on elastic foundations in thermal environments. Mech. Based Des. Struct. Mach. 54 (1), 2532734. http://dx.doi.org/10.1080/15397734.2025.2532734.

Chiang, C.M., Stiassnie, M., Yue, D.K.-P., 2005. Theory and Applications of Ocean Surface Waves. World Scientific, http://dx.doi.org/10.1142/5566.

Dean, R.G., Dalrymple, R.A., 1991. Water Wave Mechanics for Engineers and Scientists, Vol. 2, world scientific publishing company.

Ebrahimi, F., Parsi, M., 2026a. Novel heterogeneous graphene origami-enabled auxetic metabeams for high performance tunable energy harvesting. Arab. J. Sci. Eng. http://dx.doi.org/10.1007/s13369-026-11078-4.

Ebrahimi, F., Parsi, M., 2026b. Programmable energy harvesting enabled by functionally graded graphene-origami auxetic cantilever beams. J. Vib. Eng. Technol. 14 (4), 174. http://dx.doi.org/10.1007/s42417-026-02338-6.

Erturk, A., Inman, D.J., 2008a. A distributed parameter electromechanical model for cantilevered piezoelectric energy harvesters. J. Vib. Acoust. 130 (4), http://dx.doi.org/10.1115/1.2890402.

Erturk, A., Inman, D., 2008b. On mechanical modeling of cantilevered piezoelectric vibration energy harvesters. J. Intell. Mater. Syst. Struct. 19 (11), 1311–1325. http://dx.doi.org/10.1177/1045389x07085639.

Erturk, A., Inman, D.J., 2009. An experimentally validated bimorph cantilever model for piezoelectric energy harvesting from base excitations. Smart Mater. Struct. 18 (2), 025009. http://dx.doi.org/10.1088/0964-1726/18/2/025009.

Erturk, A., Vieira, W.G.R., De Marqui, J., Inman, D.J., 2010. On the energy harvesting potential of piezoaeroelastic systems. Appl. Phys. Lett. 96 (18), http://dx.doi.org/10.1063/1.3427405.

Farhangdoust, S., 2020. Auxetic cantilever beam energy harvester. SPIE Smart Structures + Nondestructive Evaluation, Vol. 11382, SPIE, http://dx.doi.org/10.1117/12.2559327.

Fey, T., Eichhorn, F., Han, G., Ebert, K., Wegener, M., Roosen, A., Kakimoto, K.-i., Greil, P., 2016. Mechanical and electrical strain response of a piezoelectric auxetic PZT lattice structure. Smart Mater. Struct. 25 (1), 015017. http://dx.doi.org/10.1088/0964-1726/25/1/015017.

Ilyas, A., Kashif, S.A.R., Saqib, M.A., Asad, M.M., 2014. Wave electrical energy systems: Implementation, challenges and environmental issues. Renew. Sustain. Energy Rev. 40, 260–268. http://dx.doi.org/10.1016/j.rser.2014.07.085.

Islam, A., Al-tabatabaie, K.F., Karmaker, A.K., Biplob Hossain, M., Islam, K., 2022. Assessing energy diversification policy and sustainability: Bangladesh standpoints. Energy Strat. Rev. 40, 100803. http://dx.doi.org/10.1016/j.esr.2022.100803.

Kepler, R.G., 1995. Ferroelectric, pyroelectric, and piezoelectric properties of poly (vinylidene fluoride). Plast. Eng.-New York- 28, 183.

Kiran, M.R., Farrok, O., Abdullah-Al-Mamun, M., Islam, M.R., Xu, W., 2020. Progress in piezoelectric material based oceanic wave energy conversion technology. IEEE Access 8, 146428–146449. http://dx.doi.org/10.1109/ACCESS.2020.3015821.

Krishnaswamy, J.A., Buroni, F.C., Melnik, R., Rodriguez-Tembleque, L., Saez, A., 2020. Design of polymeric auxetic matrices for improved mechanical coupling in lead-free piezocomposites. Smart Mater. Struct. 29 (5), 054002. http://dx.doi.org/10.1088/1361-665X/ab7e35.

Le, P.B., Do, D.N., Tran, T.T., 2026. Quasi-3D dynamic analysis of functionally graded auxetic graphene-origami-reinforced plates on viscoelastic foundations under pulse loading. Mech. Res. Commun. 153, 104643. http://dx.doi.org/10.1016/j.mechrescom.2026.104643.

Li, Q., Kuang, Y., Zhu, M., 2017. Auxetic piezoelectric energy harvesters for increased electric power output. AIP Adv. 7 (1), http://dx.doi.org/10.1063/1.4974310.

Li, Y.S., Li, S., 2025. Vibro-acoustic response and sound transmission loss of functionally graded graphene origami-enabled auxetic metamaterial plates. Acta Mech. 236 (11), 6499–6522. http://dx.doi.org/10.1007/s00707-025-04483-7.

Li, Z., Roscow, J., Khanbareh, H., Haswell, G., Bowen, C., 2024. Energy harvesting from water flow by using piezoelectric materials. Adv. Energy Sustain. Res. 5 (5), 2300235. http://dx.doi.org/10.1002/aesr.202300235.

Lian, J., Wang, X., Wang, X., Wu, D., 2024. Research on wave energy converters. Energies 17 (7), 1577. http://dx.doi.org/10.3390/en17071577.

Liu, R., He, L., Liu, X., Wang, S., Zhang, L., Cheng, G., 2023. A review of collecting ocean wave energy based on piezoelectric energy harvester. Sustain. Energy Technol. Assess. 59, 103417. http://dx.doi.org/10.1016/j.seta.2023.103417.

Liu, D., Li, Z., Kitipornchai, S., Zhao, L., Shen, X., 2026. Nonlinear buckling and postbuckling of functionally graded graphene origami-enabled auxetic metamaterial cylindrical shells under combined thermo-mechanical loads. Eng. Struct. 349, 121958. http://dx.doi.org/10.1016/j.engstruct.2025.121958.

Murari, B., Zhao, S., Zhang, Y., Ke, L., Yang, J., 2023. Vibrational characteristics of functionally graded graphene origami- enabled auxetic metamaterial beams with variable thickness in fluid. Eng. Struct. 277, 115440. http://dx.doi.org/10.1016/j.engstruct.2022.115440.

Murari, B., Zhao, S., Zhang, Y., Yang, J., 2024. Machine learning-assisted vibration analysis of graphene-origami metamaterial beams immersed in viscous fluids. Thin-Walled Struct. 197, 111663. http://dx.doi.org/10.1016/j.tws.2024.111663.

Mutsuda, H., Tanaka, Y., Doi, Y., Moriyama, Y., 2019. Application of a flexible device coating with piezoelectric paint for harvesting wave energy. Ocean Eng. 172, 170–182. http://dx.doi.org/10.1016/j.oceaneng.2018.11.014.

Na, Y.-M., Lee, H.-S., Park, J.-K., 2018. A study on piezoelectric energy harvester using kinetic energy of ocean. J. Mech. Sci. Technol. 32 (10), 4747–4755. http://dx.doi.org/10.1007/s12206-018-0922-1.

Newman, J., 1994. Wave effects on deformable bodies. Appl. Ocean Res. 16 (1), 47–59. http://dx.doi.org/10.1016/0141-1187(94)90013-2.

Nguyen, T.T.H., Nguyen, T.H., 2026. An IGA method for transient response of FG-GOEAM non-uniform thickness microplate resting on viscoelastic foundation. Int. J. Mech. Mater. Des. 22 (1), 49. http://dx.doi.org/10.1007/s10999-026-09867-8.

Pierson, Jr., W.J., Moskowitz, L., 1964. A proposed spectral form for fully developed wind seas based on the similarity theory of SA kitaigorodskii. J. Geophys. Res. 69 (24), 5181–5190. http://dx.doi.org/10.1029/JZ069i024p05181.

Qiao, D., Haider, R., Yan, J., Ning, D., Li, B., 2020. Review of wave energy converter and design of mooring system. Sustainability 12 (19), 8251. http://dx.doi.org/10.3390/su12198251.

Ramos, J.L., Pakuts, B., Godoy, P., García-Franco, A., Duque, E., 2022. Addressing the energy crisis: using microbes to make biofuels. Microb. Biotechnol. 15 (4), 1026–1030. http://dx.doi.org/10.1111/1751-7915.14050.

Reddy, J., 2003. Mechanics of Laminated Composite Plates and Shells : Theory and Analysis. CRC Press, ISBN: 9780429210693, p. 858. http://dx.doi.org/10.1201/b12409.

Ren, Z., Niu, S., Lv, A., Liu, X., Mu, W., Liu, T., Wang, Q., 2026. Bioinspired photothermal superhydrophobic metamaterial with structured micro-nano crystal arrays for anti-/de-icing. Adv. Mater. 38 (6), e16655. http://dx.doi.org/10.1002/adma.202516655.

Renzi, E., 2016. Hydroelectromechanical modelling of a piezoelectric wave energy converter. Proc. R. Soc. A: Math. Phys. Eng. Sci. 472 (2195), http://dx.doi.org/10.1098/rspa.2016.0715.

Roy Chowdhury, A., Saurabh, N., Kiran, R., Patel, S., 2021. Effect of porous auxetic structures on low-frequency piezoelectric energy harvesting systems: a finite element study. Appl. Phys. A 128 (1), 62. http://dx.doi.org/10.1007/s00339-021-05199-w.

Singh, S., 2021. Energy crisis and climate change. In: Energy. John Wiley & Sons, Ltd, ISBN: 9781119741503, pp. 1–17. http://dx.doi.org/10.1002/9781119741503.ch1.

Thorpe, T.W., 1999. A Brief Review of Wave Energy. Technical Report, Harwell Laboratory, Energy Technology Support Unit London, UK.

Topolov, V.Y., Bowen, C.R., 2015. High-performance 1–3-type lead-free piezo-composites with auxetic polyethylene matrices. Mater. Lett. 142, 265–268. http://dx.doi.org/10.1016/j.matlet.2014.12.018.

Viet, N.V., Xie, X.D., Liew, K.M., Banthia, N., Wang, Q., 2016. Energy harvesting from ocean waves by a floating energy harvester. Energy 112, 1219–1226. http://dx.doi.org/10.1016/j.energy.2016.07.019.

Vipin, V., Koley, S., 2022. Mathematical modeling of a submerged piezoelectric wave energy converter device installed over an undulated seabed. Renew. Energy 200, 1382–1392. http://dx.doi.org/10.1016/j.renene.2022.10.051.

Vu, V.T., Tran, T.T., 2025. Dynamic response analysis of FG-GOEAM plates resting on pasternak foundation under moving loads (1/4 vehicle model) considering plate surface irregularities. Ships Offshore Struct. 1–20. http://dx.doi.org/10.1080/17445302.2025.2555907.

Wang, Q., Zhong, L., Zhou, Y., Huang, G., Liu, J., Liu, H., Zhu, Q., 2026. Hierarchical cellulose nanopaper origami electronics. Carbohydr. Polymers 373, 124627. http://dx.doi.org/10.1016/j.carbpol.2025.124627.

Wegert, Z.J., Wilks, B., Thamwattana, N., Challis, V.J., Koley, S., Meylan, M.H., 2026. Wave energy conversion by floating and submerged piezoelectric bimorph plates. Ocean Eng. 354, 124792. http://dx.doi.org/10.1016/j.oceaneng.2026.124792.

Xia, Y., Zhang, B., Tao, C., Wang, L., 2025. Fully nonlinear simulation of the hydrodynamic performance of a submerged cylindrical wave energy converter in the presence of current. J. Mar. Sci. Eng. 13 (9), http://dx.doi.org/10.3390/jmse13091763.

Xie, X., Wang, Q., Wu, N., 2014. Energy harvesting from transverse ocean waves by a piezoelectric plate. Internat. J. Engrg. Sci. 81, 41–48. http://dx.doi.org/10.1016/j.ijengsci.2014.04.003.

Xie, X.D., Wang, Q., Wu, N., 2014. Potential of a piezoelectric energy harvester from sea waves. J. Sound Vib. 333 (5), 1421–1429. http://dx.doi.org/10.1016/j.jsv.2013.11.008.

Xu, J., Patel, A., Meraj, P., 2022. Impact of chronic total occlusions on outcomes of patients with acute myocardial infarction undergoing percutaneous coronary intervention: A propensity-score-matched analysis using the national inpatient sample database. Cardiovasc. Revascularization Med. 44, 14–18. http://dx.doi.org/10.1016/j.carrev.2022.06.014.

Yang, J., 2005. An Introduction to the Theory of Piezoelectricity. Springer.

Yang, J., Guo, L., Zhao, S., Yang, J., 2025a. Nonlinear damped vibrations of functionally graded graphene origami-enabled metamaterial beams with Kelvin-Voigt damping. Arch. Civ. Mech. Eng. 26 (1), 9. http://dx.doi.org/10.1007/s43452-025-01364-7.

Yang, J., Zhao, S., Yang, J., 2025b. Recent advances in graphene origami-enabled auxetic metamaterial structures. Eng. Struct. 333, 120203. http://dx.doi.org/10.1016/j.engstruct.2025.120203.

Zhang, Z., Dai, L., Wang, Z., Wu, H., 2026. Effects of WEC geometry on the performance of a WEC array-VLFS integrated system. Pol. Marit. Res. 33 (1), 63–73. http://dx.doi.org/10.2478/pomr-2026-0006.

Zhang, X., Wang, Z., Zhou, G., Li, J., Li, C., Lin, C., Xin, X., 2026. Multifunctional metamaterials based on mxene composite aerogels for integrated load-bearing and multiphysics wave attenuation. Compos. Part B: Eng. 309, 113075. http://dx.doi.org/10.1016/j.compositesb.2025.113075.

Zhao, S., Zhang, Y., Zhang, Y., Zhang, W., Yang, J., Kitipornchai, S., 2022. Genetic programming-assisted micromechanical models of graphene origami-enabled metal metamaterials. Acta Mater. 228, 117791. http://dx.doi.org/10.1016/j.actamat.2022.117791.

Zheng, S., Meylan, M., Zhang, X., Iglesias, G., Greaves, D., 2021. Performance of a plate-wave energy converter integrated in a floating breakwater. IET Renew. Power Gener. 15 (14), 3206–3219. http://dx.doi.org/10.1049/rpg2.12230.